DYNAMIC INTERACTION BETWEEN TWO INTERFACE CRACKS IN A THREE-LAYERED PLATE

Tribikram Kundu

Department of Civil Engineering and Engineering Mechanics, University of Arizona,
Tucson, AR 85721, U.S.A.

Abstract—In this paper, the dynamic interaction between two interface cracks, in a three-layered plate subjected to antiplane stress fields, is analytically studied. The problem is formulated in terms of a coupled set of integral equations, which are then solved by expanding the unknown crack opening displacements in a complete set of Chebyshev polynomials. The method is coded in a FORTRAN program and numerical results for a sample problem are presented. The results show that for the problem studied here one crack always reduces the crack opening displacement of its neighboring crack.

1. INTRODUCTION

In recent years the dynamic analysis of cracks in multilayered solid materials have received considerable attention in the literature devoted to fracture mechanics in view of the rapid increase of coated and multilayered plates in engineering applications. Investigators who studied different aspects of this problem include Loeber and Sih (1973), Keer and Luong (1974), Luong *et al.* (1975), Atkinson (1977), Srivastava *et al.* (1978), Neerhoff (1979), Sih and Chen (1980), Kuo (1982), Yang and Bogy (1985), Kundu (1986), Boström (1987), to name a few. In all these works only one crack has been considered in the problem geometry. The present state of knowledge still lacks a rigorous analytical technique for the dynamic analysis of the interaction among several interface cracks.

In this paper the transient response of two interface cracks in a multilayered plate under antiplane loading is analytically studied. Crack opening displacements (CODs) of both cracks are computed for different time-dependent loadings at the plate surface. COD is computed by both considering and neglecting the interaction effects. Comparisons between these two sets of results show how significantly a crack can affect the behavior of its neighboring crack. Since the stress intensity factor (K) is directly related to COD, exactly the same behavior would have been observed for K if it were computed instead of COD.

The analytical formulation is developed based on Betti's reciprocal theorem applied to two problem geometries, one is the scattered field problem and the other is Green's problem which is a flawless plate subjected to a concentrated line load. Thus a set of integral equations are formulated with the CODs as the unknowns. Then CODs are expanded in a complete set of Chebyshev polynomials. The unknown coefficients of these expansions are obtained by satisfying the stress free boundary conditions of the crack faces. Similar techniques were used by Neerhoff (1979), Yang and Bogy (1985), Kundu (1986) and Boström (1987) to solve wave scattering problems by a single interface crack. In the problem considered here, since there are two cracks in the problem geometry it gives rise to a set of coupled integral equations unlike the previous works with one crack only. The coupling terms represent the crack interaction effects.

2. PROBLEM FORMULATION

A plate is made of three homogeneous, isotropic, elastic layers, 1, 2 and 3, of thicknesses h_1, h_2 and h_3 as shown in Fig. 1. ρ_j and β_j are material density and shear wave velocity of the *j*th layer, respectively. Plate dimensions along the *x*- and *z*-directions are infinite. Two Griffith cracks of lengths $2a_1$ and $2a_2$ are located at the two interfaces at $y = y_1(= h_1)$ and
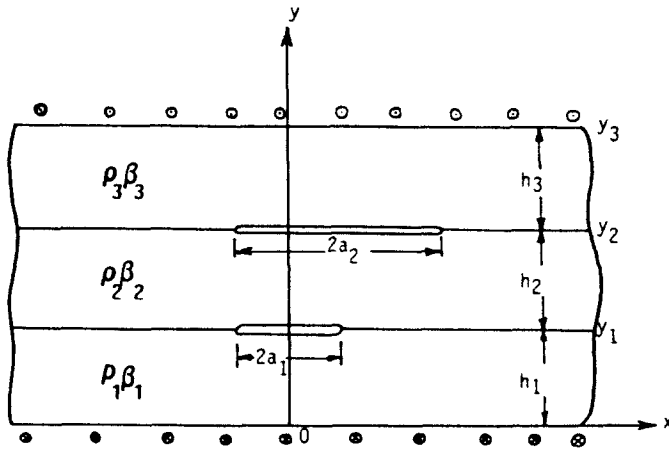
Fig. 1. Geometry of the problem. A three-layered plate containing two interface cracks is subjected to an antiplane loading.

y_2 ($= h_1 + h_2$) with a distance d between the crack centers. The two surfaces of the plate at $y = 0$ and y_3 ($= h_1 + h_2 + h_3$) are subjected to an antiplane stress field $\tau_{yz} = f(t)$ as shown in the figure. The plate and crack geometries and the surface loadings are independent of the z-direction.

To solve this problem, first we need to solve two cannonical problems. The two problems are then combined by Betti's reciprocal theorem. First the problem is solved in the frequency domain, then the transient response is obtained by Fourier inversion of the spectrum.

2.1. Cannonical problem 1 : flawless three-layered plate subjected to an antiplane stress field

The geometry of this problem is very similar to Fig. 1, the only difference is that there is no crack at any interface. The time harmonic antiplane stress field of time dependence $e^{-i\omega t}$ acts uniformly on the two surfaces of the plate. The displacement field in the jth layer of this problem geometry is given by the wave equation solution

$$U_j = A_j e^{ik_{sj} y} + B_j e^{-ik_{sj} y} \tag{1}$$

where k_{sj} is the S-wave number of the jth layer. The time dependence $e^{-i\omega t}$ in eqn (1) and in all subsequent equations is implied. The unknown coefficients A_j and B_j can be evaluated from boundary and interface conditions. Expressions of A_j and B_j are given in the Appendix.

2.2. Cannonical problem 2 : a line load in a three-layered flawless plate

The geometry of this problem is shown in Fig. 2. A time harmonic line load is acting at a point $P(x_p, y_p)$ as shown in the figure. The solution of this problem is available in the literature on wave propagations in multilayered solids (Kundu, 1986). The displacement field in the jth layer generated by this line load located at the mth layer is given by

$$U_j^G = \frac{i}{4\pi\mu_j} \int_{-\infty}^{\infty} \left\{ \delta_{mj} \frac{e^{i\eta_j |y - y_p|}}{\eta_j} + C_j e^{i\eta_j y} + D_j e^{-i\eta_j y} \right\} e^{ik(x - x_p)} dk \tag{2}$$

where

$$\eta_j = (k_{sj}^2 - k^2)^{1/2} \quad \text{for} \quad k_{sj} > k$$
$$= i(k^2 - k_{sj}^2)^{1/2} \quad \text{for} \quad k_{sj} < k \tag{3}$$

μ_j is the shear modulus of the jth layer and δ_{mj} is the Kronecker delta function which is 1 for $m = j$ and 0 for $m \neq j$.
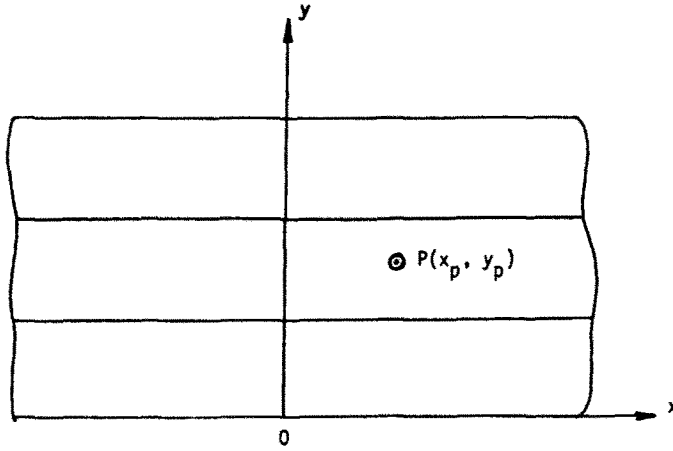
Fig. 2. A point load in the three-layered plate.

Unknown coefficients C_j and D_j can be obtained from stress-free boundary conditions and continuity conditions across the interface. Expressions of these coefficients are given in the Appendix. Superscript G on U_j indicates U_j corresponding to Green's elastodynamic state.

2.3. Application of Betti's reciprocal theorem

Let us consider two solution states S and G. State S corresponds to the scattered field of the original problem. So when S is added to the displacement field of the cannonical problem 1 the solution state of the problem of interest is obtained. The cannonical problem 2, Green's elastodynamic state, is referred to as state G. Using Betti's reciprocal theorem these two states can be related in the following manner:

$$\int_V F_i^S U_i^G \, dV + \int_S T_i^S U_i^G \, dS = \int_V F_i^G U_i^S \, dV + \int_S T_i^G U_i^S \, dS \qquad (4)$$

where F_i is the body force per unit volume acting in the x_i-direction, T_i is the surface traction per unit area acting in the x_i-direction, and U_i is the displacement in the x_i-direction. Superscripts S and G represent states S and G respectively. However, the body force for state S is zero and for state G it is equal to $\delta(\vec{r} - \vec{r}_p)$ acting in the z-direction. $\vec{r}_p$ is the position vector of point P and $\vec{r}$ is the position vector of any point of interest. For an antiplane problem all non-zero forces and displacements act in the z-direction. So for our problem the general equation, eqn (4), takes the form

$$\int_S T^S U^G \, dS = U^S(\vec{r}_p) + \int_S T^G U^S \, dS \qquad (5)$$

where U is the particle displacement and T is the shear stress. Since the problem is invariant in the z-direction, surface integrals may be reduced to line integrals. This line integral is carried out along a contour, shown in Fig. 3.

The integral on the left-hand side of eqn (5) vanishes because T^S is zero on C_1, C_2, C_3, C_4 and the integrals of $T^S U^G$ on Σ_j^+ and Σ_j^- cancel each other for $j = 1$ and 2. The only non-zero term comes from the integral on the right-hand side of eqn (5) along the integration paths Σ_j^+ and Σ_j^-. After some simplification, eqn (5) is reduced to

$$U^S(\vec{r}_p) = \int_{-a_1}^{a_1} \phi(x) T^G \, dx + \int_{d-a_2}^{d+a_2} \psi(x-d) T^G \, dx \qquad (6)$$

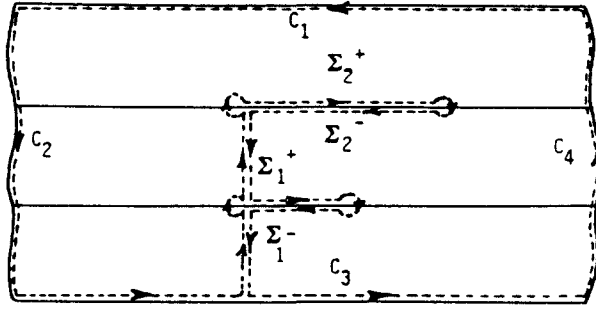where $\phi(x)$ and $\psi(x)$ are CODs of the two cracks and are defined as

Fig. 3. Contour of the line integral (eqn (5)).

$$\phi(x) = U^S(x, y_1^+) - U^S(x, y_1^-)$$
$$\psi(x) = U^S(x, y_2^+) - U^S(x, y_2^-).$$

(7)

The expressions for T^G at $y = y_1$ and y_2 may be obtained from

$$T^G(x, y_1) = T_1^G(x, y_1^-) = T_2^G(x, y_1^+) = \mu_2 \left\{ \frac{\partial U_2^G}{\partial y} \right\}_{y=y_1}$$

(8a)

and

$$T^G(x, y_2) = T_2^G(x, y_2^-) = T_1^G(x, y_2^+) = \mu_2 \left\{ \frac{\partial U_2^G}{\partial y} \right\}_{y=y_2}$$

(8b)

where U_2^G is given in eqn (2).

If point P is now taken on the crack surface, the displacement of that point can be obtained from eqn (6) if T_G, $\phi(x)$ and $\psi(x)$ are known. Combining eqns (6) and (8) the displacement field at x_p, y_p ($y_p = y_1$ or y_2) is obtained

$$U_2^S(x_p, y_p) = \frac{1}{4\pi} \int_{-a_1}^{a_1} \phi(x) \int_{-\infty}^{\infty} \{e^{i\eta_2(y_p - y_1)} - \eta_2(C_2 - D_2)\} e^{ik(x - x_p)} \, dk \, dx$$

$$- \frac{1}{4\pi} \int_{d-a_2}^{d+a_2} \psi(x) \int_{-\infty}^{\infty} \{e^{i\eta_2(y_2 - y_p)} + \eta_2(C_2 Q_2 - D_2 Q_2^{-1})\} e^{ik(x - x_p)} \, dk \, dx$$

(9)

where

$$Q_2 = e^{i\eta_2 h_2}.$$

The scattered stress field can be obtained from the displacement field of eqn (9). Then it is equated to the negative of the incident stress field along the crack surfaces ($y = y_1$, $|x| < a_1$ and $y = y_2$, $|X| < a_2$, $X = x - d$) to obtain

$$k_{12}(A_2 - B_2) = \frac{1}{4\pi} \int_{-a_1}^{a_1} \phi(x) \int_{-\infty}^{\infty} F_1(k) e^{ik(x - x_p)} \, dk \, dx$$

$$+ \frac{1}{4\pi} \int_{-a_2}^{a_2} \psi(X) \int_{-\infty}^{\infty} F_2(k) e^{ik(X - x_p) + ikd} \, dk \, dX \quad \text{for} \quad -a_1 < x_p < a_1 \quad (10a)$$

and

$$k_{,2}(A_2 Q_2 - B_2 Q_2^{-1}) = \frac{1}{4\pi} \int_{-a_1}^{a_1} \phi(x) \int_{-\infty}^{\infty} F_3(k) \, e^{ik(x - X_p) - ikd} \, dk \, dx$$

$$+ \frac{1}{4\pi} \int_{-a_2}^{a_2} \psi(X) \int_{-\infty}^{\infty} F_4(k) \, e^{ik(X - X_p)} \, dk \, dX \quad \text{for} \quad -a_2 < X_p < a_2 \quad (10b)$$

where

$$F_1(k) = -\eta_2 \left\{ 1 + i \frac{\partial}{\partial y_p} (C_2 - D_2) \right\}_{y_p = y_1}$$

$$F_2(k) = -\eta_2 \left\{ Q_2 + i \frac{\partial}{\partial y_p} (C_2 Q_2 - D_2 Q_2^{-1}) \right\}_{y_p = y_1}$$

$$\qquad\qquad\qquad\qquad\qquad\qquad\qquad\qquad\qquad (11)$$

$$F_3(k) = -\eta_2 \left\{ Q_2 + i \frac{\partial}{\partial y_p} (C_2 - D_2) \right\}_{y_p = y_2}$$

$$F_4(k) = -\eta_2 \left\{ 1 + i \frac{\partial}{\partial y_p} (C_2 Q_2 - D_2 Q_2^{-1}) \right\}_{y_p = y_2}$$

A_2, B_2 in eqns (10) and C_2, D_2 in eqns (11) are defined in eqns (1) and (2), respectively. Partial derivatives of C_2 and D_2 with respect to y_p at $y_p = y_1$ and y_2 are given in the Appendix.

It can be shown that $F_j(k)$, ($j = 1, 2, 3, 4$) is imaginary for all real values of k. It can also be shown that $F_2(k)$ is always equal to $F_3(k)$ and they approach zero as $k \to \infty$. However, $F_1(k)$ and $F_4(k)$ have the following asymptotic expressions:

$$\lim_{k \to \infty} F_1(k) = -\frac{2ik\mu_1}{\mu_1 + \mu_2}$$

$$\qquad\qquad\qquad\qquad\qquad\qquad\qquad\qquad\qquad (12)$$

$$\lim_{k \to \infty} F_4(k) = -\frac{2ik\mu_3}{\mu_2 + \mu_3}.$$

It should be noted here that the integrals involving $F_2(k)$ and $F_3(k)$ represent the interaction effects between the two cracks. In the coupled integral equations, eqns (10), the functions $\phi(x)$ and $\psi(x)$ are yet unknown.

2.4. Computation of the crack opening displacement functions

In order to evaluate the CODs, $\phi(x)$ and $\psi(x)$ are expanded in a complete set of Chebyshev polynomials

$$\phi(x) = \sum_{n=0}^{\infty} \left[\frac{\alpha_{2n}}{2n} \phi_{2n}(x) + i \frac{\alpha_{2n+1}}{2n+1} \phi_{2n+1}(x) \right]$$

$$\qquad\qquad\qquad\qquad\qquad\qquad\qquad\qquad\qquad (13)$$

$$\psi(x) = \sum_{n=0}^{\infty} \left[\frac{\gamma_{2n}}{2n} \psi_{2n}(x) + i \frac{\gamma_{2n+1}}{2n+1} \psi_{2n+1}(x) \right]$$

where

$$\phi_{2n}(x) = \sin \{2n \arcsin (x/a_1)\}$$

$$\psi_{2n}(x) = \sin \{2n \arcsin (x/a_2)\} \qquad\qquad\qquad (14)$$

$$\phi_{2n+1}(x) = \cos \{(2n+1) \arcsin (x/a_1)\}$$

$$\psi_{2n+1}(x) = \cos \{(2n+1) \arcsin (x/a_2)\}.$$

To obtain the unknown coefficients α_n and γ_n, both sides of eqn (10a) are multiplied by $\phi_m(x_p)$, then integrated from $x_p = -a_1$ to a_1 and both sides of eqn (10b) are multiplied by $\psi_m(x_p)$, then integrated from $X_p = -a_2$ to a_2. After some algebraic manipulation an infinite set of linear equations is obtained to solve for α_n and γ_n

$$\sum_{n=1}^{\infty} (K_{mn}\alpha_n + L_{mn}\gamma_n) = -2ik_{s2}(A_2 - B_2)a_1\delta_{m1}$$

$$\sum_{n=1}^{\infty} (M_{mn}\alpha_n + N_{mn}\gamma_n) = -2ik_{s2}(A_2Q_2 - B_2Q_2^{-1})a_2\delta_{m1}$$

(15)

where for $m+n = $ even

$$K_{mn} = 2\int_0^{\infty} \left\{ \frac{F_1(k)}{k^2} + \frac{2i\mu_1}{k(\mu_1+\mu_2)} \right\} J_m(ka_1)J_n(ka_1)\ dk - \frac{2i\mu_1}{\mu_1+\mu_2}\frac{\delta_{mn}}{m}$$

$$L_{mn} = 2\int_0^{\infty} \frac{F_2(k)}{k^2} J_m(ka_1)J_n(ka_2)\ \cos\ (kd)\ dk$$

(16)

$$M_{mn} = 2\int_0^{\infty} \frac{F_2(k)}{k^2} J_m(ka_2)J_n(ka_1)\ \cos\ (kd)\ dk$$

$$N_{mn} = 2\int_0^{\infty} \left\{ \frac{F_4(k)}{k^2} + \frac{2i\mu_3}{k(\mu_2+\mu_3)} \right\} J_m(ka_2)J_n(ka_2)\ dk - \frac{2i\mu_3}{\mu_2+\mu_3}\frac{\delta_{mn}}{m}$$

and for $m+n = $ odd

$$K_{mn} = N_{mn} = 0$$

$$L_{mn} = 2i\int_0^{\infty} \frac{F_2(k)}{k^2} J_m(ka_1)J_n(ka_2)\ \sin\ (kd)\ dk$$

(17)

$$M_{mn} = -2i\int_0^{\infty} \frac{F_2(k)}{k^2} J_m(ka_2)J_n(ka_1)\ \sin\ (kd)\ dk.$$

From eqns (16) and (17) it can be clearly seen that K and N matrices are symmetric but the L and M matrices are not. However, L and M satisfy the following relations:

$$L_{mn} = \begin{cases} M_{nm} & \text{for}\quad m+n = \text{even} \\ -M_{nm} & \text{for}\quad m+n = \text{odd}. \end{cases}$$

Equations (15) have infinite series in their expressions, however, they can be terminated after a finite number of terms without introducing any significant error. Then α_n, γ_n can be obtained from a finite set of linear equations and finally $\phi(x)$ and $\psi(x)$ can be computed from eqns (13) without any difficulty.

3. COMPUTATIONAL ASPECTS

The main task involved in obtaining the solution of this problem is the computation of the integral expressions of K_{mn}, L_{mn}, M_{mn} and N_{mn}. The major difficulty in computing these integrals comes from the fact that a finite number of poles or singular points lie on the real path of integration. These correspond to the roots of the denominator of the integrands. This denominator is the surface wave dispersion function of the problem geometry. These poles are removed from the complicated integral expressions in the same

manner as done in a previous paper (Kundu, 1986). Then the poles are confined to relatively simpler integrals having the following forms:

$$I = \int_0^\infty \frac{J_m(ka_i)J_n(ka_i)}{k^2 - p^2}\, dk, \quad i = 1 \text{ or } 2 \tag{18}$$

$$I_c = \int_0^\infty \frac{J_m(ka_i)J_n(ka_j)\, \cos\,(kd)}{k^2 - p^2}\, dk, \quad i,j = 1,2 \text{ or } 2,1\,; \quad i \neq j \tag{19}$$

$$I_s = \int_0^\infty \frac{J_m(ka_i)J_n(ka_j)\, \sin\,(kd)}{k^2 - p^2}\, dk, \quad i,j = 1,2 \text{ or } 2,1\,; \quad i \neq j \tag{20}$$

where p is a pole of the integrand on the real k-axis. Integrals in eqn (18) have been evaluated (Kundu, 1986)

$$\int_0^\infty \frac{J_m(ka_i)J_n(ka_i)}{k^2 - p^2}\, dk = \begin{cases} \dfrac{\pi i}{2p} H_m^{(1)}(pa_i)J_n(pa_i), & m \leqslant n \\[2ex] \dfrac{\pi i}{2p} H_n^{(1)}(pa_i)J_m(pa_i), & m \geqslant n \end{cases} \tag{21}$$

where $H_m^{(1)}$ is the Hankel function of first kind of order m.

Let us now try to evaluate the integrals of eqn (19). It was shown (Kundu, 1986) that for $m \geqslant n$, $J_m(ka)H_n^{(i)}(ka)$ vanishes at $k = 0$ for both $i = 1$ and 2. So for $m \geqslant n$ the numerator of the integrand of eqn (19) can be written as

$$\tfrac{1}{4}[H_m^{(1)}(ka_i) + H_m^{(2)}(ka_i)]J_n(ka_j)\,[e^{ikd} + e^{-ikd}]. \tag{22}$$

Clearly for large k, $H_m^{(1)}(ka_i)\, e^{ikd} = O(e^{ik(a_i+d)})$, so it goes to zero when k takes large positive imaginary values. Similarly $H_m^{(2)}\, e^{-ikd}$ becomes zero when k takes large negative imaginary values. So integrals containing $H_m^{(1)}\, e^{ikd}$ can be evaluated by the contour integration method closing the contour in the first quadrant and integrands containing $H_m^{(2)} e^{-ikd}$ should be closed in the fourth quadrant. But the term $H_m^{(1)}(ka_i)\, e^{-ikd} = O(e^{ik(a_i-d)})$ for large k, so contours of the integrals containing these terms should be closed in the first quadrant if $a_i > d$ and in the fourth quadrant if $a_i < d$. Following the same logic the contours of the integrals containing $H_m^{(2)}(ka_i)\, e^{ikd}$ should be closed in the first quadrant if $a_i < d$ and in the fourth quadrant if $a_i > d$. If $m \leqslant n$, J_n (instead of J_m) should be expressed in terms of Hankel functions and then those expressions can be integrated by the contour integration method as discussed above. Integrals of eqn (20) can also be evaluated following the same technique. Final results of these contour integrations are given below

$$I_c = i(I_1 + I_2 + I_3)$$
$$I_s = I_1 + I_2 - I_3 \tag{23}$$

where, for $m \geqslant n$

$$I_1 = \frac{\pi}{4p} J_m(pa_i)H_n^{(1)}(pa_j)\, e^{ipd} \tag{24a}$$

$$I_2 = \begin{cases} 0 & \text{for } a_j > d \\[2ex] \dfrac{\pi}{4p} J_m(pa_i)H_n^{(2)}(pa_j)\, e^{ipd} & \text{for } a_j < d \end{cases} \tag{24b}$$

Table 1. Material properties and dimensions of the specimen

Layer number	Layer material	Thickness, h (mm)	Density, ρ (g cm^{-1})	S-Wave speed, β (km s^{-1})
1	Copper	0.5	8.9	2.32
2	Steel	0.5	7.9	3.20
3	Quartz	0.5	2.2	3.77

$$I_3 = \begin{cases} \dfrac{\pi}{4p} J_m(pa_i)H_n^{(1)}(pa_i)\, e^{-ipd} & \text{for} \quad a_i > d \\ 0 & \text{for} \quad a_i < d \end{cases} \tag{24c}$$

and for $m \leqslant n$

$$I_1 = \frac{\pi}{4p} J_n(pa_i)H_m^{(1)}(pa_i)\, e^{ipd} \tag{25a}$$

$$I_2 = \begin{cases} 0 & \text{for} \quad a_i > d \\ \dfrac{\pi}{4p} J_n(pa_i)H_m^{(2)}(pa_i)\, e^{ipd} & \text{for} \quad a_i < d \end{cases} \tag{25b}$$

$$I_3 = \begin{cases} \dfrac{\pi}{4p} J_n(pa_i)H_m^{(1)}(pa_i)\, e^{-ipd} & \text{for} \quad a_i > d \\ 0 & \text{for} \quad a_i < d. \end{cases} \tag{25c}$$

4 RESULTS

The method discussed above has been implemented in a FORTRAN program. Results for a sample case are presented in this section. The plate specimen for which numerical results are given is made of copper, steel and quartz. A 2 mm crack is located at the copper steel interface and a second crack of length 4 mm is located at the quartz steel interface. The distance between the centers of the two cracks is 0.5 mm. Properties of the plate materials are given in Table 1.

In the results presented in Figs 4 8, length, time and frequency units are in mm, μs and MHz, respectively.

The poles of the integrands on the real k-axis are shown in Fig. 4. It should be noted here that the number of poles increases with increasing frequency and so does the computing cost.

Profiles of CODs for different exciting frequencies are shown in Fig. 5. The rate of convergence of the proposed method can be observed in this figure. α_n and γ_n of eqn (13)
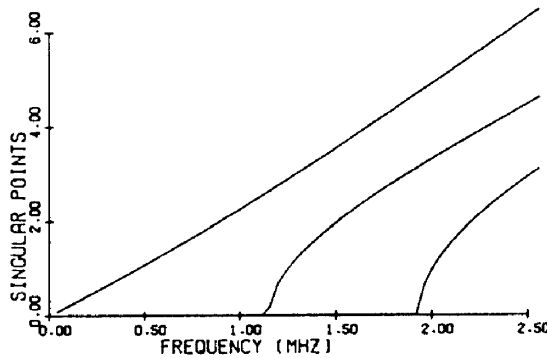

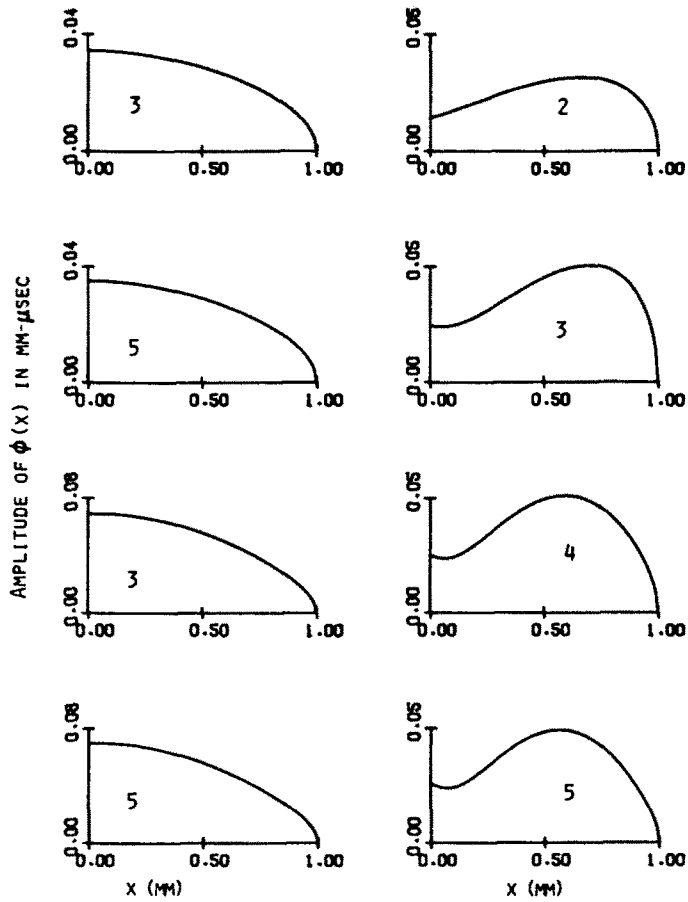Fig. 4. Singular points on the real k-axis of integration as a function of frequency.

Fig. 5. Spectral amplitudes (in mm-μs) of crack opening displacements of the 2 mm long crack at different exciting frequencies. Left-hand column: the top two figures are for 0.04 MHz and the bottom two figures are for 0.6 MHz exciting frequencies. Right-hand column: all four figures are for 1 MHz frequency. The number in each figure indicates the number of terms considered in the series expansion of $\phi(x)$ in eqns (13).
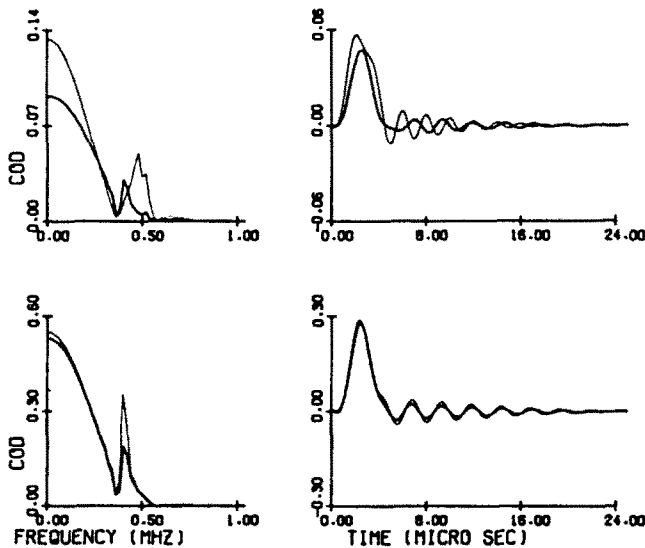

Fig. 6. Crack opening displacements at the center of the crack for the impact loading (eqn (26)) with duration $\tau = 5$ μs. The top row is for the 2 mm crack and the bottom row is for the 4 mm crack. Left-hand column: COD spectral amplitudes in mm-μs. Right-hand column: COD time histories in mm. In each figure the bold curve represents the actual COD and the thin curve represents the COD of the same crack in the absence of the other crack.
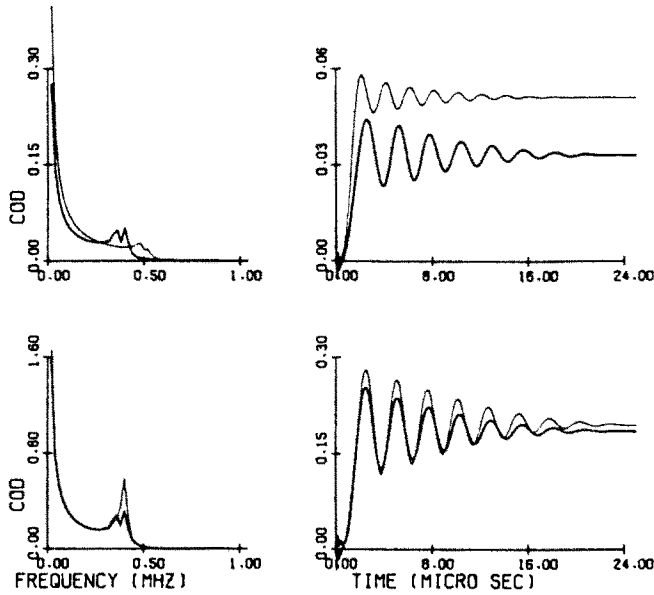
Fig. 7. Same as Fig. 6 but the applied load is a step load (eqn (28)) with rise time $\tau 2 = 2.5 \mu s$.

are obtained by solving eqns (15). Logically, it may be stated that a large number of terms in the expansion of CODs $\phi(x)$ and $\psi(x)$ should give accurate results. But then the size of the K, L, M and N matrices increases and so does the computing cost. However, it can be seen in Fig. 5 that it is not necessary to consider more than five terms in the COD expansion for frequencies up to 1 MHz. In the top two figures of the left-hand column of Fig. 5 the amplitude of the COD $\phi(x)$ is plotted for an exciting frequency of 0.04 MHz. The top figure is for a three-term expansion and the second figure, for a five-term expansion. The bottom two figures of the left-hand column show the amplitude of $\phi(x)$ for three- and five-term expansions at a frequency of 0.6 MHz. Clearly for both these frequencies the three-term expansion of $\phi(x)$ can produce accurate results. In the right-hand column the COD $\phi(x)$ is plotted for a frequency of 1 MHz for two-, three-, four-, and five-term expansions of $\phi(x)$. For this frequency it can be said that after four- or five-term expansions the result converges. Similar convergence is observed for $\psi(x)$. For all plots of Fig. 5, the Fourier transform $F(\omega)$ of the exciting load has been equated to 1.
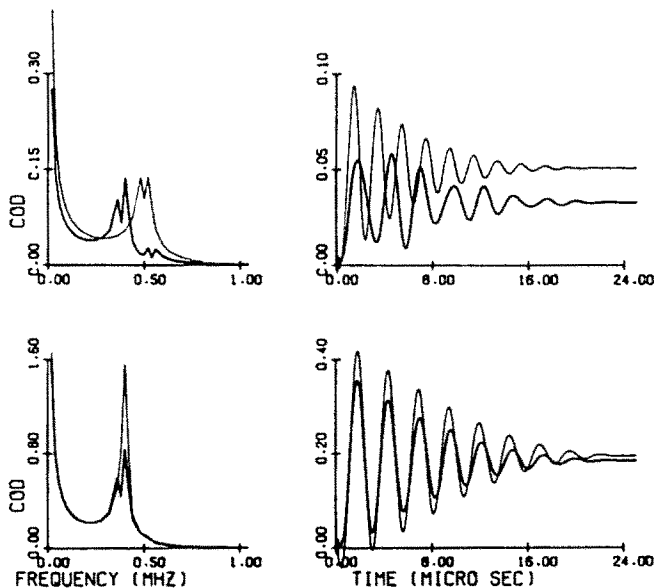

Fig. 8. Same as Fig. 7 but the rise time $(\tau/2)$ of the step load is 1 μs.

The response of the two cracks to impact and step loadings are shown in Figs 6–8. For impact loading the load starts from zero, then reaches a peak value and finally drops down to zero. In step loading the load starts from zero and gradually attains a maximum value. The following functions are considered as loading functions.

Impact loading

$$f(t) = \begin{cases} 16Pt^2(t-\tau)^2\tau^{-4}, & 0 \leqslant t \leqslant \tau \\ 0, & t \geqslant \tau \end{cases} \tag{26}$$

$$F(\omega) = \frac{32P}{\tau^4\omega^3}\left[\left\{-\frac{6\tau}{\omega} + i\left(\tau^2 - \frac{12}{\omega^2}\right)\right\}e^{i\omega\tau} - \left\{\frac{6\tau}{\omega} + i\left(\tau^2 - \frac{12}{\omega^2}\right)\right\}\right]. \tag{27}$$

Step loading

$$f(t) = \begin{cases} 16Pt^2(t-\tau)^2\tau^{-4}, & 0 \leqslant t \leqslant \tau/2 \\ P, & t \geqslant \tau/2 \end{cases} \tag{28}$$

$$F(\omega) = \frac{16P}{\tau^4}\left[\frac{\tau^4}{16}\pi\delta(\omega) - \frac{i}{\omega^3}\left(\tau^2 + \frac{24}{\omega^2}\right)e^{i\omega\tau/2} + \frac{2}{\omega^3}\left\{i\left(\frac{12}{\omega^2} - \tau^2\right) - \frac{6\tau}{\omega}\right\}\right]. \tag{29}$$

In the above equations P defines the peak value of the plate surface excitation stress. In subsequent calculations, P is set equal to 1 kN mm^{-2}. τ is the duration of the impact load. The sharpness of the impact can be increased by decreasing τ but keeping P constant. The rise time of the step load is equal to $\tau/2$. Here too a sharp rise in loading can be modeled by decreasing τ but keeping P constant. Results are given for $\tau = 5$ and 2 μs.

In eqn (29) $F(\omega)$ is not suitable for numerical evaluation because it contains a delta function and a singular term which behaves like $1/\omega$ near $\omega = 0$. This difficulty is avoided by separating the static part and shifting the response history vertically as discussed by Mal et al. (1984).

In Figs 6–8 CODs at the center of the 2 and 4 mm cracks are plotted in the top and bottom rows, respectively. Displacement spectra are plotted in the left-hand column and time histories in the right-hand column. Time histories are obtained numerically by inverting the response spectra using FFT (fast Fourier transform) routine. In all these figures two curves are plotted, one with a bold pen and the other with a thin pen. The bold curves are actual plots of COD and the thin curves are the COD plots when the interaction between the two cracks is neglected. In other words thin curves represent the response of one crack when the other crack is absent. They are obtained by setting the coupling matrices L and M equal to a null matrix.

In Fig. 6 COD for the impact load with duration $\tau = 5$ μs is shown. The difference between the thick and thin curves is more for the 2 mm crack (top row) than the 4 mm crack (bottom row). It is justified since the effect of the larger crack on the smaller crack should be more than the effect of the smaller crack on the larger crack. In the time history plot of the top row it can be seen that in approximately 11 μs the bold curve oscillates three times and the thin curve oscillates four times. The presence of the second crack reduces the stiffness of the plate and hence the natural frequency of vibration of the crack opening is reduced. It can also be seen that the maximum crack opening increases when the interaction effect is neglected. So for the model studied here, the presence of the second crack reduces the possibility of the propagation of the first crack.

The response of the two cracks for step type of loading with rise time $\tau/2 = 2.5$ μs is shown in Fig. 7. Here again the bold curves represent the actual response and the thin curves represent the crack response in the absence of the other crack. Here also the greater difference between the two curves is observed for the smaller crack. In the top row in about 10 μs the thick curve oscillates three times and the thin curve oscillates four times. Thus

the decrease in stiffness and natural frequency in the presence of the second crack can be observed in this figure also. The presence of the second crack significantly reduces the maximum COD of the smaller crack. Another interesting feature of the top figure should be observed here, the bold curve oscillates for a longer period of time than the thin curve. It is probably due to the fact that the free surfaces of the second crack restricts to some extent the geometric dissipation of energy from the first crack.

Figure 8 is similar to Fig. 7, the only difference here is that the rise time for the step load is 1 μs instead of 2.5 μs. Hence the dynamic effect in this figure is more than that in Fig. 7. Other observations, i.e. differences in the plate stiffness and COD magnitudes, in the presence and absence of the second crack are similar to the previous figure.

5. CONCLUSION

In this paper the interactions between two interface cracks in a three-layered plate is studied analytically, when the plate is subjected to a time-dependent antiplane shear stress field. This new technique is an extension of the technique used to solve the single interface crack problem (Kundu, 1986). The method developed here is found to be very efficient, quickly converging to a negligible error.

A sample problem involving two interface cracks in a three-layered plate is solved by this technique. The numerical results show that the dynamic reponse of a crack is significantly influenced by the presence of a neighboring crack if the neighboring crack is longer. For the plate model studied here it is found that the presence of one crack always reduces the COD of its neighboring crack.

REFERENCES

Atkinson, C. (1977). Dynamic crack problems in dissimilar media. In *Mechanics of Fracture* (Edited by G. C. Sih), Vol. 4, pp. 213–248. Noordhoff, Leyden.

Boström, A. (1987). Elastic wave scattering from an interface crack : antiplane strain. *ASME J. Appl. Mech.* 54, 503–508 (1987).

Keer, L. M. and Luong, W. C. (1974). Diffraction of waves and stress intensity factors in a cracked layered composite. *J. Acoust. Soc. Am.* 56, 1681–1686.

Kundu, T. (1986). Transient response of an interface crack in a layered plate. *ASME J. Appl. Mech.* 53, 579–586.

Kuo, A.-Y. (1982). Dynamic analysis of interfacial cracks in composite laminates. Ph.D. dissertation, Department of Theoretical and Applied Mechanics, University of Illinois at Urbana-Champaign.

Loeber, J. F. and Sih, G. C. (1973). Transmission of anti-plane shear waves past an interface crack in dissimilar media. *Engng Fracture Mech.* 5, 699–725.

Luong, W. C., Keer, L. M. and Achenbach, J. D. (1975). Elastodynamic stress intensity factors of a crack near an interface. *Int. J. Solids Structures* 11, 919–925.

Mal, A. K., Kundu, T. and Xu, P.-C. (1984). On the surface response of a multilayered solid to a dislocation source. *Proceedings of the ASME Conference on Earthquake Source Modeling, Ground Motion and Structural Response*, San Antonio, Texas (Edited by S. K. Datta), PVP-Vol. 80, pp. 29–48. ASME United Engineering Center, New York.

Neerhoff, F. L. (1979). Diffraction of Love waves by a stress-free crack of finite width in the plane interface of a layered composite. *Appl. Scient. Res.* 35, 265–315.

Sih, G. C. and Chen, E. P. (1980). Normal and shear impact of layered composite with a crack : dynamic stress intensification. *ASME J. Appl. Mech.* 47, 351–358.

Srivastava, K. N., Gupta, O. P. and Palaiya, R. M. (1978). Interaction of elastic waves in two dissimilar elastic half-planes having Griffith crack at interface—I. *Int. J. Fracture* 14, 145–154.

Yang, H. J. and Bogy, D. B. (1985). Elastic wave scattering from an interface crack in a layered half-space. *ASME J. Appl. Mech.* 52, 42–50.

APPENDIX

Expressions of A_j, B_j, C_j and D_j ($j = 1, 2, 3$) of eqns (1) and (2) are given here. Partial derivatives of C_2 and D_2 with respect to y_p (see eqns (11)) are also defined here

$$A_3 = \frac{F(\omega)}{ip_1\beta_1\omega}\left(\frac{1+gq_1P_{13}}{f+gq_1^2}\right)$$

$$B_3 = \frac{F(\omega)}{ip_1\beta_1\omega}\left(\frac{q_1-fP_{13}}{f+gq_1^2}\right)$$

$$A_2 = \frac{1}{2q_2}\{A_3(1+P_{32})+B_3(1-P_{32})\} \tag{A1}$$

$$B_2 = \frac{q_2}{2}\{A_3(1-P_{32})+B_3(1+P_{32})\}$$

$$A_1 = \frac{1}{2q_1}\{A_2(1+P_{21})+B_2(1-P_{21})\}$$

$$B_1 = \frac{q_1}{2}\{A_2(1-P_{21})+B_2(1+P_{21})\}$$

where

$$q_i = \exp(ik_{ri}h_i)$$

$$P_{ij} = \frac{k_{ri}\mu_i}{k_{rj}\mu_j}$$

$$f = \frac{1}{4q_1q_2}\{(1-q_1^2)[(1+q_2^2)+P_{12}(1-q_2^2)]+P_{21}(1+q_1^2)[(1-q_2^2)+P_{12}(1+q_2^2)]\}$$

$$g = \frac{1}{4q_1q_2}\{(1-q_1^2)[(1+q_2^2)-P_{12}(1-q_2^2)]+P_{21}(1+q_1^2)[(1-q_2^2)-P_{12}(1+q_2^2)]\}. \tag{A2}$$

$F(\omega)$ is the Fourier transform of the applied stress field on the plate boundary and ω is the frequency. p_i, β_i, μ_i, and k_{ri} are defined in the text.

Now C_i and D_i of eqn (2) are defined as

$$C_2 = \frac{F_1-F_2}{\eta_2 M}\{(F_1-F_4)p_2Q_2-(F_1+F_4)P_2\}$$

$$D_2 = Q_2\frac{F_1-F_4}{\eta_2 M}\{(F_1-F_2)P_2Q_2-(F_1+F_2)p_2\} \tag{A3}$$

$$C_1 = D_1 = \frac{\eta_2 Q_1}{\eta_1(Q_1^2-1)}\left(C_2-D_2-\frac{p_2}{\eta_2}\right)$$

$$C_1 = D_1Q_1^{-2} = \frac{\eta_2}{\eta_1(1-Q_1^2)}\left(C_2Q_2-D_2Q_2^{-1}+\frac{p_2}{\eta_2}\right)$$

where

$$M = (F_1+F_2)(F_1+F_4)-Q_2^2(F_1-F_2)(F_1-F_4)$$

$$F_1 = \mu_1\eta_1(1-Q_1^2)$$

$$F_2 = \mu_2\eta_2(1+Q_1^2)$$

$$F_3 = \mu_1\eta_1(1-Q_2^2) \tag{A4}$$

$$F_4 = \mu_2\eta_2(1+Q_2^2)$$

$$P_2 = e^{\eta_2(y_p-y_2)}$$

$$p_2 = e^{\eta_2(y_2-y_p)}$$

$$Q_i = e^{\eta_i h_i}$$

η_i is defined in eqn (3).

Partial derivatives of C_2 and D_2 with respect to y_p have the following forms:

$$\frac{\partial C_2}{\partial y_p} = -\frac{i}{M}(F_1-F_2)\{p_2Q_2(F_1-F_4)+P_2(F_1+F_4)\}$$

$$\frac{\partial D_2}{\partial y_p} = \frac{i}{M}(F_1-F_4)\{P_2Q_2(F_1-F_2)+p_2(F_1+F_2)\} \tag{A5}$$

where M, F_1, F_2, F_3, F_4, Q_2, P_2 and p_2 are defined in eqns (A4). Clearly if $y_p = y_1$ then $P_2 = 1$, $p_2 = Q_2$ and if $y_p = y_2$ then $P_2 = Q_2$, $p_2 = 1$.